A combined VPT and SVT approach for decoupling in the presence of inaccessible and deformable interfaces

M. Di Manno [1], **F. Trainotti** [2], **M. Ialonardi** [1], **D. J. Rixen** [2], **A. Fregolent** [1]
[1] Università degli Studi di Roma La Sapienza, Dipartimento di Ingegneria Meccanica e Aerospaziale, Via Eudossiana, 18, Roma, Italy

[2] Technical University of Munich, School of Engineering and Design, Chair of Applied Mechanics, Boltzmannstrasse, 15, Garching, Germany

Abstract
Substructure decoupling identifies a subsystem within a mechanical system by removing the measured dynamics of other subsystems from that of the assembly. Challenges persist in this procedure in the presence of inaccessible and flexible interfaces, measurement errors and noise. Various approaches address these issues: the Virtual Point Transformation (VPT) reduces noise at boundary DoFs but fails to capture the interface flexibility. The extended decoupling interface can help to overcome this limitation by involving internal DoFs in the decoupling but leads to major error propagation. The Singular Vector Transformation (SVT) reduces errors at internal DoFs but lacks a physical description of the interface. This work proposes different approaches to decoupling that combine VPT, the extended interface, and SVT to retain the interface flexibility and to smooth measurement errors at all DoFs while describing the interface topology with physical coordinates. Advantages are demonstrated on a laboratory benchmark structure using experimental data.

1 Introduction

In the context of frequency-based substructuring [1], substructure decoupling is particularly useful for identifying the dynamic behavior of subsystems that are part of a larger mechanical system but are difficult to model or experimentally characterize individually. Different types of decoupling methods are available in literature [2–4]. The one defined within the Lagrange Multiplier - Frequency Based Substructuring (LM-FBS) [5], also known as dual substructure decoupling [6, 7], identifies the unknown subsystem by removing the dynamics of the remaining (residual) subsystem from that of the assembly. In this case, the subsystems involved are characterized by their Frequency Response Functions (FRFs), which correspond to the interface DoFs (DoFs between which the subsystems are connected in the assembled configuration) and to the internal DoFs (not belonging to the interface). Compatibility and equilibrium conditions need to be imposed on the DoFs shared between the assembly and the residual subsystem. Unlike coupling procedures, where these conditions can only be imposed on the interface DoFs, dual decoupling allows to define different types of interfaces [8–10]. The most straightforward are the standard (interface DoFs only) and the extended (interface and internal DoFs) interfaces. However, challenges remain in accurately performing decoupling when dealing with inaccessible and flexible interfaces between components, as well as in the presence of measurement error and noise. In these cases, the FRFs at the interface DoFs (translational and rotational) cannot be directly measured and must be retrieved using other techniques. One technique commonly used for this task is the Virtual Point Transformation (VPT) [11], that reduces the measured dynamics at some boundary DoFs near the interface using a set of generalized coordinates associated with six rigid Interface Deformation Modes (IDMs). These generalized coordinates can be thought of as the physical translational and rotational coordinates of a virtual point placed in the inaccessible interface region. A side advantage of this technique is that it helps mitigate the presence of measurement noise. In performing decoupling, compatibility and equilibrium conditions can now be imposed only on the set of rigid interface dynamics. In this sense, the decoupling compatibility conditions are said to be weakened [12, 13], i.e. they are imposed on a reduced

subspace where only the dynamics relevant for the decoupling are represented, in a least-squares sense. Consequently, weakening the decoupling by the VPT prevents the dynamics of the flexible interface from being captured. To overcome this problem, the extended decoupling interface can be helpful. In fact, including a set of measured internal DoFs in the decoupling process improves the controllability and observability of the flexible interface dynamics. However, errors at the internal DoFs are not mitigated and may propagate into the solution. Another approach commonly used to weaken interface compatibility conditions is the Singular Vector Transformation (SVT) [14]. Here, decoupling is performed in a reduced space extracted from direct measurements at the interface and internal DoFs. These DoFs are distributed to fully control and observe the interface dynamics. The SVT helps to mitigate errors at all measured DoFs while retaining the flexible interface dynamics. The drawback of this approach is that the interface is now represented by generalized singular coordinates, i.e. the topology described by the physical translational and rotational coordinates is lost. This can be a limitation in some applications, e.g. joint identification or where a direct physical attachment enables a simple/interpretable connection between components.

In this work, different approaches to weaken the interface compatibility conditions are tested. They combine the concepts of VPT, the extended decoupling interface and of the SVT approaches. The overall advantage is that the improved controllability/observability of the flexible interface dynamics is ensured by the extended interface concept, while the measurement errors are smoothed both at the interface and at the internal DoFs. In addition, the interface topology described by the translational and rotational coordinates is maintained and represented by the virtual point DoFs. The effectiveness of the proposed solutions over state-of-the-art methods is evaluated on a laboratory benchmark structure using experimental data.

2 Theoretical background

This Section describes the theoretical background of standard (Section 2.1) and weakened (Section 2.2) dual decoupling. Two common approaches to weaken compatibility conditions, the Virtual Point Transformation (VPT) and the Singular Vector Transformation (SVT), are described in Sections 2.3 and 2.4, respectively.

2.1 Dual substructure decoupling

The dual decoupling [6, 9], allows to identify the dynamic behavior of an unknown mechanical subsystem U starting from the known FRFs $\mathbf{Y}^{\mathrm{RU}}$ of an assembled mechanical system RU containing U and the known FRFs $\mathbf{Y}^{\mathrm{R}}$ of the remaining (residual) subsystems R (see Fig. 1). In the following, it is considered that the FRFs (accelerances) of the residual subsystem R are known on three different sets of DoFs, reported in Fig. 1: the interface DoFs c, between which R and U are connected in the assembled configuration; the boundary DoFs b, which are close to the interface and are able to control/observe all its dynamics; the internal DoFs i, which do not belong to the interface region. Note that the DoFs b will not be directly used in the coupling or decoupling of the substructures, but will be exploited to approximate the behavior at the interface, as explained later (e.g. Fig. 2). Similarly, the FRFs of the assembled system are defined on the same DoFs of RU, plus a set of DoFs v representing the internal DoFs of the unknown subsystem that

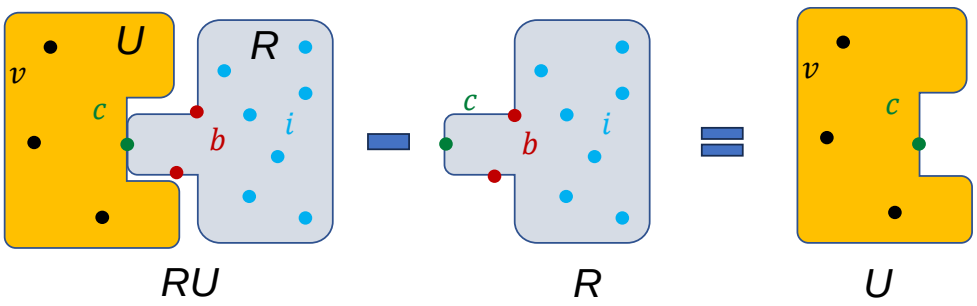

Figure 1: Dual substructuring procedure to identify the dynamic behaviour of the unknown subsystem U.

cannot be measured when disassembled. In the LM-FBS framework, decoupling is performed starting from the uncoupled equations of motion of the assembled system and of a fictitious subsystem with an FRF matrix opposite in sign to that of the residual subsystem:

$$\boldsymbol{u} = \mathbf{Y}(\boldsymbol{f} + \boldsymbol{g}) \quad \Leftrightarrow \quad \begin{Bmatrix} \boldsymbol{u}^{\mathrm{RU}} \\ \boldsymbol{u}^{\mathrm{R}} \end{Bmatrix} = \begin{bmatrix} \mathbf{Y}^{\mathrm{RU}} & \mathbf{0} \\ \mathbf{0} & -\mathbf{Y}^{\mathrm{R}} \end{bmatrix} \left(\begin{Bmatrix} \boldsymbol{f}^{\mathrm{RU}} \\ \boldsymbol{f}^{\mathrm{R}} \end{Bmatrix} + \begin{Bmatrix} \boldsymbol{g}^{\mathrm{RU}} \\ \boldsymbol{g}^{\mathrm{R}} \end{Bmatrix} \right) \tag{1}$$

where $\mathbf{Y}$ is the FRF matrix of the subsystems to be decoupled in block diagonal format, $\boldsymbol{u}$ is the response vector, $\boldsymbol{f}$ is the vector of the externally applied forces, $\boldsymbol{g}$ is the vector of disconnection forces between RU and R. To perform decoupling in the dual approach, compatibility (strictly enforced) and equilibrium (automatically satisfied) conditions must be imposed between some DoFs shared by RU and R. This is done using the signed Boolean matrices $\mathbf{B}_{\mathrm{u}}$ and $\mathbf{B}_{\mathrm{f}}$ as follows:

$$\begin{cases} \mathbf{B}_{\mathrm{u}} \boldsymbol{u} = \mathbf{0} \\ \boldsymbol{g} = -{\mathbf{B}_{\mathrm{f}}}^{T} \boldsymbol{\lambda} \end{cases} \tag{2}$$

where $\boldsymbol{\lambda}$ are the Lagrange multipliers that represent the disconnection force intensities. The set of DoFs on which compatibility and equilibrium conditions are imposed forms what is called the decoupling interface. The most basic one contains only the interface DoFs c (standard interface). However, one can use the so-called extended interface, where these compatibility and equilibrium conditions are imposed on both interface c and internal i DoFs. Solving the system of equations formed by Eq. (1) and (2) results in the following one-line equation:

$$\boldsymbol{u} = \left[\mathbf{Y} - \mathbf{Y}{\mathbf{B}_{\mathrm{f}}}^{T} \left(\mathbf{B}_{\mathrm{u}} \mathbf{Y} {\mathbf{B}_{\mathrm{f}}}^{T} \right)^{+} \mathbf{B}_{\mathrm{u}} \mathbf{Y} \right] \boldsymbol{f} = \overline{\mathbf{Y}}^{\mathrm{U}} \boldsymbol{f} \tag{3}$$

where $\bar{\mathbf{Y}}^{\mathrm{U}}$ is the FRF matrix of the identified unknown subsystem and $(\cdot)^{+}$ indicates the Moore-Penrose pseudo-inverse operator. Care must be taken when inverting the matrix product $\mathbf{B}_{\mathrm{u}} \mathbf{Y} {\mathbf{B}_{\mathrm{f}}}^{T}$, also called the Interface Flexibility Matrix (IFM), because it can lead to large error propagation if it is ill-conditioned and measurements are affected by errors and noise. Note that only some elements of $\bar{\mathbf{Y}}^{\mathrm{U}}$ should be retained. In particular, those corresponding to the DoFs belonging to the unknown subsystem, i.e. the interface DoFs c and the internal DoFs v of U.

2.2 Weakened dual decoupling

In many applications, the FRFs at the interface DoFss c cannot be measured directly. Moreover, the presence of measurement noise may affect the result of the decoupling. To deal with these applications, one possible way is to weaken the compatibility conditions [9, 11, 12]. Compatibility and equilibrium conditions are imposed using the signed Boolean matrices $\tilde{\mathbf{B}}_{\mathbf{u}}$ and $\tilde{\mathbf{B}}_{\mathbf{f}}$, which operate in the reduced subspaces as follows:

$$\begin{cases} \tilde{\mathbf{B}}_{\mathbf{q}} \boldsymbol{q} = \tilde{\mathbf{B}}_{\mathbf{q}} {\mathbf{R}_{\mathrm{u}}}^{+} \boldsymbol{u} = \mathbf{0} \\ \boldsymbol{g} = -({\mathbf{R}_{\mathrm{f}}}^{+})^{H} {\tilde{\mathbf{B}}_{\mathbf{m}}}^{T} \boldsymbol{\lambda}_{\mathrm{m}} \end{cases} \tag{4}$$

where the matrices $\mathbf{R}_{\mathrm{u}}$ and $\mathbf{R}_{\mathrm{f}}$ reduce the physical displacements and forces to the sets of generalized responses $\boldsymbol{q}$ and forces $\boldsymbol{m}$ as follows:

$$\begin{cases} \boldsymbol{u} = \mathbf{R}_{\mathrm{u}} \boldsymbol{q} + \boldsymbol{\mu} \\ \boldsymbol{m} = {\mathbf{R}_{\mathrm{f}}}^{H} \boldsymbol{g} \end{cases} \tag{5}$$

where $\boldsymbol{\mu}$ are the remaining responses living outside the reduced subspace and $(\cdot)^{H}$ denotes the complex conjugate transpose operator, since in general $\mathbf{R}_{\mathrm{u}}$ and $\mathbf{R}_{\mathrm{f}}$ are complex-valued and frequency-dependent matrices. Note that the compatibility as written in Eq. (4) expresses an approximate compatibility, since it is enforced in a reduced space where only the interface dynamics relevant to the decoupling are represented in a least-squares sense. Instead, the residual dynamics, which carry the effects of unwanted dynamics, noise, and measurement error, are allowed to be incompatible. In this case, it is not strictly necessary to measure

directly at the interface DoFs, but only to perform measurements close enough to the interface to allow for the control/observation of its relevant dynamics.
Several methods, with different advantages/disadvantages, can be found in the literature to weaken the compatibility conditions. They differ mainly in the construction of the matrices $\mathbf{R}_\mathrm{u}$ and $\mathbf{R}_\mathrm{f}$ used for the response and force reductions. To compare different approaches, these two matrices can be written in block diagonal form to show how the reductions are performed separately on RU and R, and on their distinct sets of DoFs (see the DoF partitioning in section 2.1):

$$\mathbf{R}_\mathrm{u} = \begin{bmatrix} \mathbf{I}_{vv}^{RU} & & & & \\ & \mathbf{R}_{u,ii}^{RU} & & & \\ & & \mathbf{R}_{u,cc}^{RU} & & \\ & & & \mathbf{R}_{u,ii}^{R} & \\ & & & & \mathbf{R}_{u,cc}^{R} \end{bmatrix} \qquad \mathbf{R}_\mathrm{f} = \begin{bmatrix} \mathbf{I}_{vv}^{RU} & & & & \\ & \mathbf{R}_{f,ii}^{RU} & & & \\ & & \mathbf{R}_{f,ii}^{RU} & & \\ & & & \mathbf{R}_{f,ii}^{R} & \\ & & & & \mathbf{R}_{f,cc}^{R} \end{bmatrix} \tag{6}$$

where $\mathbf{I}_{vv}^{RU}$ is an identity matrix indicating that the internal DoFs v of the unknown subsystem are not reduced.

2.3 Virtual Point Transformation

The Virtual Point Transformation (VPT) [11] can be seen as a way to weaken the compatibility conditions. This technique reduces responses and forces at the boundary DoFs b of a subsystem using the transformation bases $\mathbf{R}_{u,bb}^{RU}$ and $\mathbf{R}_{f,bb}^{R}$, which are formed by a set of rigid Interface Deformation Modes (IDMs). In general, these bases are frequency independent, since they depend only on the geometry of the subsystem and the orientation of the sensors. The generalized coordinates associated with the IDMs can be thought of as the translational and rotational DoFs of a virtual point (VP) located at the interface, and thus play the role of the interface DoFs. An example of displacement reduction is shown in Fig. 2. Overall, the displacement and

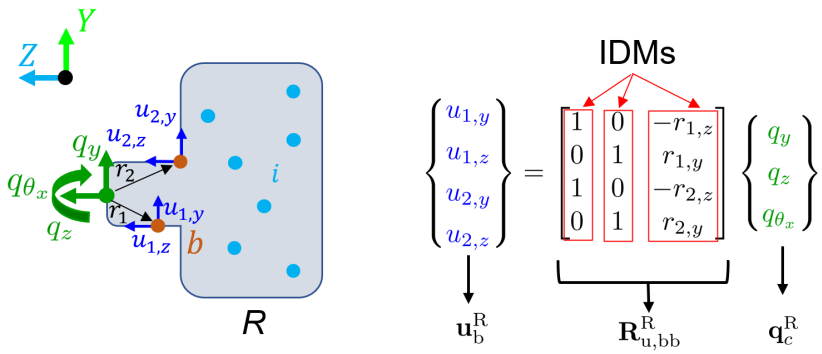

Figure 2: Example of virtual point displacement transformation on subsystem R. The displacements at the boundary DoFs b are reduced to three virtual point displacements q_y, q_z and q_{θ_x}, associated to three rigid IDMs. These play the role of the coupling DoFs.

force reductions in Eq. (5) take the following form:

$$\begin{Bmatrix} \boldsymbol{u}_{\mathrm{v}}^{\mathrm{RU}} \\ \boldsymbol{u}_{\mathrm{i}}^{\mathrm{RU}} \\ \boldsymbol{u}_{\mathrm{b}}^{\mathrm{RU}} \\ \boldsymbol{u}_{\mathrm{i}}^{\mathrm{R}} \\ \boldsymbol{u}_{\mathrm{b}}^{\mathrm{R}} \end{Bmatrix} = \begin{bmatrix} \mathbf{I}_{\mathrm{vv}}^{\mathrm{RU}} & & & & \\ & \mathbf{I}_{\mathrm{ii}}^{\mathrm{RU}} & & & \\ & & \mathbf{R}_{\mathrm{u,bb}}^{\mathrm{RU}} & & \\ & & & \mathbf{I}_{\mathrm{ii}}^{\mathrm{R}} & \\ & & & & \mathbf{R}_{\mathrm{u,bb}}^{\mathrm{R}} \end{bmatrix} \begin{Bmatrix} \boldsymbol{u}_{\mathrm{v}}^{\mathrm{RU}} \\ \boldsymbol{u}_{\mathrm{i}}^{\mathrm{RU}} \\ \boldsymbol{q}_{\mathrm{b}}^{\mathrm{RU}} \\ \boldsymbol{u}_{\mathrm{i}}^{\mathrm{R}} \\ \boldsymbol{q}_{\mathrm{b}}^{\mathrm{R}} \end{Bmatrix} + \begin{Bmatrix} \mathbf{0} \\ \mathbf{0} \\ \boldsymbol{\mu}_{\mathrm{b}}^{\mathrm{RU}} \\ \mathbf{0} \\ \boldsymbol{\mu}_{\mathrm{b}}^{\mathrm{R}} \end{Bmatrix}$$
$$\begin{Bmatrix} \boldsymbol{g}_{\mathrm{v}}^{\mathrm{RU}} \\ \boldsymbol{g}_{\mathrm{i}}^{\mathrm{RU}} \\ \boldsymbol{m}_{\mathrm{b}}^{\mathrm{RU}} \\ \boldsymbol{g}_{\mathrm{i}}^{\mathrm{R}} \\ \boldsymbol{m}_{\mathrm{b}}^{\mathrm{R}} \end{Bmatrix} = \begin{bmatrix} \mathbf{I}_{\mathrm{vv}}^{\mathrm{RU}} & & & & \\ & \mathbf{I}_{\mathrm{ii}}^{\mathrm{RU}} & & & \\ & & \mathbf{R}_{\mathrm{f,bb}}^{\mathrm{RU}} & & \\ & & & \mathbf{I}_{\mathrm{ii}}^{\mathrm{R}} & \\ & & & & \mathbf{R}_{\mathrm{f,bb}}^{\mathrm{R}} \end{bmatrix}^{T} \begin{Bmatrix} \boldsymbol{g}_{\mathrm{v}}^{\mathrm{RU}} \\ \boldsymbol{g}_{\mathrm{i}}^{\mathrm{RU}} \\ \boldsymbol{g}_{\mathrm{b}}^{\mathrm{RU}} \\ \boldsymbol{g}_{\mathrm{i}}^{\mathrm{R}} \\ \boldsymbol{g}_{\mathrm{b}}^{\mathrm{R}} \end{Bmatrix} \tag{7}$$

The VPT has the advantage that the interface topology is described in terms of physical translational and rotational coordinates, making it easy to connect or disconnect the subsystem with adjacent ones. Moreover, by weakening the compatibility conditions (Eq. (4)) through the VPT, the measurement noise at the boundary DoFs contained in the residual motion $\boldsymbol{\mu}_{\mathrm{b}}^{\mathrm{RU}}$ and $\boldsymbol{\mu}_{\mathrm{b}}^{\mathrm{R}}$, remains incompatible. The drawback is that the VPT does not account for the flexible motion of the interface that is not involved in the decoupling. The combination of the VPT with the extended decoupling interface can help to overcome this problem, since the inclusion of internal DoFs in the IFM improves the observability/controllability of the deformable dynamics [8, 9, 15]. However, this approach is generally affected by large error propagation, since redundant dynamics can enter the IFM (thus worsening its conditioning) together with measurement errors and noise present at the internal DoFs (which is not filtered).

2.4 Singular Vector Transformation

Another possible approach to weaken the dual decoupling problem is to use the Singular Vector Transformation (SVT), as proposed in [14]. An important requirement for using this approach is that the response points in both R and RU are at the same position. This also applies to the excitation points. The SVT reduces the responses and forces at internal and boundary DoFs using common reduction bases. These bases are extracted from the experimental measurements of the residual subsystem by performing the SVD, e.g. [16], on the FRF matrix $\mathbf{Y}_{\mathrm{rr}}^{\mathrm{R}}$:

$$\mathbf{Y}_{\mathrm{rr}}^{\mathrm{R}}(\omega) = \mathbf{U}^{\mathrm{R}}(\omega)\boldsymbol{\Sigma}^{\mathrm{R}}(\omega)\left(\mathbf{V}^{\mathrm{R}}(\omega)\right)^{H} \tag{8}$$

where r denotes the set of internal and boundary DoFs, i.e., $r = i \cup b$. The columns of $\mathbf{U}^{\mathrm{R}}$ and $\mathbf{V}^{\mathrm{R}}$ are the frequency dependent left and right complex singular vectors of $\mathbf{Y}_{\mathrm{rr}}^{\mathrm{R}}$, respectively. They carry the information of the interface deformation and have the property of being orthogonal. The matrix $\boldsymbol{\Sigma}^{\mathrm{R}}$ contains the singular values σ of $\mathbf{Y}_{\mathrm{rr}}^{\mathrm{R}}$, which indicates the relevance of the associated singular vectors to the dynamics of the subsystem. By examining the frequency distribution of the singular values, also called the Complex Mode Indicator Function (CMIF) plot, a reduced number k of significant singular values can be selected along with the corresponding set of k singular vectors $\mathbf{U}^{\mathrm{R,k}}$ and $\mathbf{V}^{\mathrm{R,k}}$. These truncated sets are then used to reduce the responses and forces of both the residual and the assembled systems as follows:

$$\begin{Bmatrix} \boldsymbol{u}_{\mathrm{v}}^{\mathrm{RU}} \\ \boldsymbol{u}_{\mathrm{r}}^{\mathrm{RU}} \\ \boldsymbol{u}_{\mathrm{r}}^{\mathrm{R}} \end{Bmatrix} = \begin{bmatrix} \mathbf{I}_{\mathrm{vv}}^{\mathrm{RU}} & & \\ & \mathbf{U}^{\mathrm{R,k}} & \\ & & \mathbf{U}^{\mathrm{R,k}} \end{bmatrix} \begin{Bmatrix} \boldsymbol{u}_{\mathrm{v}}^{\mathrm{RU}} \\ \boldsymbol{q}_{\mathrm{r}}^{\mathrm{RU}} \\ \boldsymbol{q}_{\mathrm{r}}^{\mathrm{R}} \end{Bmatrix} + \begin{Bmatrix} \mathbf{0} \\ \boldsymbol{\mu}_{\mathrm{r}}^{\mathrm{RU}} \\ \boldsymbol{\mu}_{\mathrm{r}}^{\mathrm{R}} \end{Bmatrix}$$
$$\begin{Bmatrix} \boldsymbol{g}_{\mathrm{v}}^{\mathrm{RU}} \\ \boldsymbol{m}_{\mathrm{r}}^{\mathrm{RU}} \\ \boldsymbol{m}_{\mathrm{r}}^{\mathrm{R}} \end{Bmatrix} = \begin{bmatrix} \mathbf{I}_{\mathrm{vv}}^{\mathrm{RU}} & & \\ & \mathbf{V}^{\mathrm{R,k}} & \\ & & \mathbf{V}^{\mathrm{R,k}} \end{bmatrix}^{H} \begin{Bmatrix} \boldsymbol{g}_{\mathrm{v}}^{\mathrm{RU}} \\ \boldsymbol{g}_{\mathrm{r}}^{\mathrm{RU}} \\ \boldsymbol{g}_{\mathrm{r}}^{\mathrm{R}} \end{Bmatrix} \tag{9}$$

where the $\boldsymbol{q}_\mathrm{r}$ are the generalized singular coordinates associated with the k retained singular vectors, while $\boldsymbol{\mu}_\mathrm{r}$ contains the dynamics associated with the low singular values and carries the effects of redundant measurements and errors present in the data.
Weakening the compatibility conditions (Eq. (4)) by SVT allows to retain flexible interface dynamics while avoiding direct measurements at the interface DoFs and averaging measurement errors/noise at both internal and boundary DoFs. Interestingly, the reduction bases are frequency dependent, allowing the analyst some leeway in constructing the best bases for efficiently describing the dynamics of the subsystems frequency by frequency.
Despite the advantages of SVT, the reduced generalized coordinates at the interface lack physical interpretability, making operations such as joint identification and coupling with other substructures difficult.

3 Proposed new bases for weakening

In this Section, several approaches to weaken the interface compatibility conditions of decoupling are proposed.

3.1 VPT and SVT

In the first proposed approach, the VPT is used to reduce the dynamics at the boundary DoFs b to the virtual point (interface) DoFs, while the SVT is used to reduce the dynamics at the internal DoFs i. The internal transformation is performed using a reduced frequency dependent basis extracted from the SVD of $\mathbf{Y}^\mathrm{R}_\mathrm{ii}(\omega)$

$$\mathbf{Y}^\mathrm{R}_\mathrm{ii}(\omega) = \tilde{\mathbf{U}}^\mathrm{R}(\omega)\tilde{\mathbf{\Sigma}}^\mathrm{R}(\omega)(\tilde{\mathbf{V}}^\mathrm{R}(\omega))^H \tag{10}$$

by considering only the k singular vectors $\tilde{\mathbf{U}}^{\mathrm{R,k}}$ and $\tilde{\mathbf{U}}^{\mathrm{R,k}}$ associated with the largest k singular values. It follows that the displacements and force reductions in Eq. (5) take the form below:

$$\begin{Bmatrix} \boldsymbol{u}^\mathrm{RU}_\mathrm{v} \\ \boldsymbol{u}^\mathrm{RU}_\mathrm{i} \\ \boldsymbol{u}^\mathrm{RU}_\mathrm{b} \\ \boldsymbol{u}^\mathrm{R}_\mathrm{i} \\ \boldsymbol{u}^\mathrm{R}_\mathrm{b} \end{Bmatrix} = \begin{bmatrix} \mathbf{I}^\mathrm{RU}_\mathrm{vv} & & & & \\ & \tilde{\mathbf{U}}^{\mathrm{R,k}} & & & \\ & & \mathbf{R}^\mathrm{RU}_\mathrm{u,bb} & & \\ & & & \tilde{\mathbf{U}}^{\mathrm{R,k}} & \\ & & & & \mathbf{R}^\mathrm{R}_\mathrm{u,bb} \end{bmatrix} \begin{Bmatrix} \boldsymbol{u}^\mathrm{RU}_\mathrm{v} \\ \boldsymbol{q}^\mathrm{RU}_\mathrm{i} \\ \boldsymbol{q}^\mathrm{RU}_\mathrm{b} \\ \boldsymbol{q}^\mathrm{R}_\mathrm{i} \\ \boldsymbol{q}^\mathrm{R}_\mathrm{b} \end{Bmatrix} + \begin{Bmatrix} \mathbf{0} \\ \boldsymbol{\mu}^\mathrm{RU}_\mathrm{i} \\ \boldsymbol{\mu}^\mathrm{RU}_\mathrm{b} \\ \boldsymbol{\mu}^\mathrm{R}_\mathrm{i} \\ \boldsymbol{\mu}^\mathrm{R}_\mathrm{b} \end{Bmatrix}$$
$$\begin{Bmatrix} \boldsymbol{g}^\mathrm{RU}_\mathrm{v} \\ \boldsymbol{m}^\mathrm{RU}_\mathrm{i} \\ \boldsymbol{m}^\mathrm{RU}_\mathrm{b} \\ \boldsymbol{m}^\mathrm{R}_\mathrm{i} \\ \boldsymbol{m}^\mathrm{R}_\mathrm{b} \end{Bmatrix} = \begin{bmatrix} \mathbf{I}^\mathrm{RU}_\mathrm{vv} & & & & \\ & \tilde{\mathbf{V}}^{\mathrm{R,k}} & & & \\ & & \mathbf{R}^\mathrm{RU}_\mathrm{f,bb} & & \\ & & & \tilde{\mathbf{V}}^{\mathrm{R,k}} & \\ & & & & \mathbf{R}^\mathrm{R}_\mathrm{f,bb} \end{bmatrix}^H \begin{Bmatrix} \boldsymbol{g}^\mathrm{RU}_\mathrm{v} \\ \boldsymbol{g}^\mathrm{RU}_\mathrm{i} \\ \boldsymbol{g}^\mathrm{RU}_\mathrm{b} \\ \boldsymbol{g}^\mathrm{R}_\mathrm{s} \\ \boldsymbol{g}^\mathrm{R}_\mathrm{b} \end{Bmatrix} \tag{11}$$

Decoupling is then performed by imposing compatibility and equilibrium conditions on the virtual point DoFs and on the retained singular coordinates k (extended decoupling interface). The overall advantage of this approach is that the improved controllability/observability of the flexible interface dynamics is ensured by the extended interface concept, while measurement errors on both the boundary and internal dynamics are smoothed. Furthermore, the interface topology is described by the physical translational and rotational coordinates associated with the virtual point, which makes later coupling of the identified part U with another substructure easy. Note that a similar method could be defined by reducing the internal DoFs i with a rigid VPT instead of the SVT. However, the SVT is preferred here to retain the internal flexible dynamics.

3.2 VPT and partitioned SVT

The second approach proposed to weaken the compatibility conditions is a slight modification of the one proposed in Section 3.1. The difference is that the internal responses and forces are reduced using a small set of p singular vectors, this time extracted from measurements performed on both the internal and boundary DoFs, i.e. coming from Eq. (8). More specifically, the restriction of the first p singular vectors $\mathbf{U}^{\mathrm{R,p}}$ and $\mathbf{V}^{\mathrm{R,p}}$ to the internal DoFs i is considered, i.e., $\mathbf{U}_{\mathrm{i}}^{\mathrm{R,p}}$ and $\mathbf{V}_{\mathrm{i}}^{\mathrm{R,p}}$, respectively. The displacement and force reductions in Eq. (5) then take the form below:

$$\begin{aligned}
\begin{Bmatrix} \boldsymbol{u}_{\mathrm{v}}^{\mathrm{RU}} \\ \boldsymbol{u}_{\mathrm{i}}^{\mathrm{RU}} \\ \boldsymbol{u}_{\mathrm{b}}^{\mathrm{RU}} \\ \boldsymbol{u}_{\mathrm{i}}^{\mathrm{R}} \\ \boldsymbol{u}_{\mathrm{b}}^{\mathrm{R}} \end{Bmatrix} &= \begin{bmatrix} \mathbf{I}_{\mathrm{vv}}^{\mathrm{RU}} & & & & \\ & \mathbf{U}_{\mathrm{i}}^{\mathrm{R,p}} & & & \\ & & \mathbf{R}_{\mathrm{u,bb}}^{\mathrm{RU}} & & \\ & & & \mathbf{U}_{\mathrm{i}}^{\mathrm{R,p}} & \\ & & & & \mathbf{R}_{\mathrm{u,bb}}^{\mathrm{R}} \end{bmatrix} \begin{Bmatrix} \boldsymbol{u}_{\mathrm{v}}^{\mathrm{RU}} \\ \boldsymbol{q}_{\mathrm{i}}^{\mathrm{RU}} \\ \boldsymbol{q}_{\mathrm{b}}^{\mathrm{RU}} \\ \boldsymbol{q}_{\mathrm{i}}^{\mathrm{R}} \\ \boldsymbol{q}_{\mathrm{b}}^{\mathrm{R}} \end{Bmatrix} + \begin{Bmatrix} \mathbf{0} \\ \boldsymbol{\mu}_{\mathrm{i}}^{\mathrm{RU}} \\ \boldsymbol{\mu}_{\mathrm{b}}^{\mathrm{RU}} \\ \boldsymbol{\mu}_{\mathrm{i}}^{\mathrm{R}} \\ \boldsymbol{\mu}_{\mathrm{b}}^{\mathrm{R}} \end{Bmatrix} \\
\begin{Bmatrix} \boldsymbol{g}_{\mathrm{v}}^{\mathrm{RU}} \\ \boldsymbol{m}_{\mathrm{i}}^{\mathrm{RU}} \\ \boldsymbol{m}_{\mathrm{b}}^{\mathrm{RU}} \\ \boldsymbol{m}_{\mathrm{i}}^{\mathrm{R}} \\ \boldsymbol{m}_{\mathrm{b}}^{\mathrm{R}} \end{Bmatrix} &= \begin{bmatrix} \mathbf{I}_{\mathrm{vv}}^{\mathrm{RU}} & & & & \\ & \mathbf{V}_{\mathrm{i}}^{\mathrm{R,p}} & & & \\ & & \mathbf{R}_{\mathrm{f,bb}}^{\mathrm{RU}} & & \\ & & & \mathbf{V}_{\mathrm{i}}^{\mathrm{R,p}} & \\ & & & & \mathbf{R}_{\mathrm{f,bb}}^{\mathrm{R}} \end{bmatrix}^{H} \begin{Bmatrix} \boldsymbol{g}_{\mathrm{v}}^{\mathrm{RU}} \\ \boldsymbol{g}_{\mathrm{i}}^{\mathrm{RU}} \\ \boldsymbol{g}_{\mathrm{b}}^{\mathrm{RU}} \\ \boldsymbol{g}_{\mathrm{s}}^{\mathrm{R}} \\ \boldsymbol{g}_{\mathrm{b}}^{\mathrm{R}} \end{Bmatrix}
\end{aligned} \tag{12}$$

Again, within the decoupling, compatibility and equilibrium conditions are imposed on the set of virtual point DoFs and on the retained p singular coordinates. With respect to the approach in Section 3.1, this should further mitigate the presence of noise at the internal DoFs, since the singular vectors used for displacement and force reduction at these DoFs are extracted from a richer dataset (measurements at b and i DoFs instead of just at i DoFs).

3.3 VPT and orthogonalized SVT

Both approaches proposed in Sections 3.1 and 3.2 can help mitigate the noise on the boundary and internal FRFs involved in the extended interface. However, including internal DoFs in the decoupling interface may introduce redundant dynamics into the interface problem. In fact, if the rigid motion is well captured by the interface DoFs using their IDMs, then the rigid body motion of the internal DoFs would already be adequately represented by the VPT. Thus, the basic idea of the approach proposed here is to introduce into the interface problem only the deformable behavior of the internal DoFs to improve the controllability/observability of the dynamics not captured by the VPT. This is achieved by constructing reduction bases for the displacement and force transformations at the internal DoFs that represent only their deformable behavior. In this regard, a VPT is performed on the residual subsystem R to reduce the responses and forces at the internal DoFs i, to the virtual point DoFs. The transformation matrices $\mathbf{R}_{\mathrm{u,ii}}^{\mathrm{R}}$ and $\mathbf{R}_{\mathrm{f,ii}}^{\mathrm{R}}$ are constructed, which rigidly span the subspaces of the internal response and the forces, respectively, by 6 IDMs. Next, the transformation basis $\mathbf{R}_{\mathrm{u,ii}}^{\mathrm{R}}$ and the full set of singular vectors $\tilde{\mathbf{U}}^{\mathrm{R}}(\omega)$ extracted from the FRFs $\mathbf{Y}_{\mathrm{ii}}^{\mathrm{R}}(\omega)$ are stacked column-wise in a matrix $\mathbf{A}$:

$$\mathbf{A} = \left[\mathbf{R}_{\mathrm{u,ii}}^{\mathrm{R}} \,\middle|\, \tilde{\mathbf{U}}^{\mathrm{R}}(\omega) \right] \tag{13}$$

The QR decomposition is applied to $\mathbf{A}$ to extract a set of orthonormal vectors that span its column space:

$$\mathbf{Q}_{\mathrm{u}}\mathbf{R} = \mathbf{A} \qquad \Rightarrow \qquad \left[\mathbf{Q}_{\mathrm{u}}^{\mathrm{rigid}} \,\middle|\, \mathbf{Q}_{\mathrm{u}}^{\mathrm{def}}(\omega) \right] \mathbf{R} = \mathbf{A} \tag{14}$$

Note that the first six vectors $\mathbf{Q}_{\mathrm{u}}^{\mathrm{rigid}}$ obtained are frequency independent and form an orthonormal basis for the 6 rigid IDMs of VPT[1], while the remaining vectors $\mathbf{Q}_{\mathrm{u}}^{\mathrm{def}}(\omega)$ are frequency dependent. These last vectors

[1]The classical VPT rigid IDMs do not form an orthogonal set because they have the property of being orthogonal with respect to the mass and stiffness matrices of the system.

form an orthonormal basis for the flexible motion of the internal DoFs i, which lies outside the space spanned by $\mathbf{Q}_{\mathrm{u}}^{\mathrm{rigid}}$. The same is done for the internal forces:

$$\mathbf{B} = \left[\mathbf{R}_{\mathrm{f,ii}}^{\mathrm{R}} \middle| \tilde{\mathbf{V}}^{\mathrm{R}}(\omega) \right] \qquad \Rightarrow \qquad \left[\mathbf{Q}_{\mathrm{f}}^{\mathrm{rigid}} \middle| \mathbf{Q}_{\mathrm{f}}^{\mathrm{def}}(\omega) \right] \hat{\mathbf{R}} = \mathbf{B} \tag{15}$$

To exclude the rigid internal dynamics from the decoupling process, the responses and forces at these DoFs are reduced using a subset s of the deformable representation vectors $\mathbf{Q}_{\mathrm{u}}^{\mathrm{def}}(\omega)$ and $\mathbf{Q}_{\mathrm{f}}^{\mathrm{def}}(\omega)$, i.e. $\mathbf{Q}_{\mathrm{u}}^{\mathrm{def,s}}(\omega)$ and $\mathbf{Q}_{\mathrm{f}}^{\mathrm{def,s}}(\omega)$. The displacement and force reductions in Eq. 5 then take the form below:

$$\begin{Bmatrix} \boldsymbol{u}_{\mathrm{v}}^{\mathrm{RU}} \\ \boldsymbol{u}_{\mathrm{i}}^{\mathrm{RU}} \\ \boldsymbol{u}_{\mathrm{b}}^{\mathrm{RU}} \\ \boldsymbol{u}_{\mathrm{i}}^{\mathrm{R}} \\ \boldsymbol{u}_{\mathrm{b}}^{\mathrm{R}} \end{Bmatrix} = \begin{bmatrix} \mathbf{I}_{\mathrm{vv}}^{\mathrm{RU}} & & & & \\ & \mathbf{Q}_{\mathrm{u}}^{\mathrm{def,s}} & & & \\ & & \mathbf{R}_{\mathrm{u,bb}}^{\mathrm{RU}} & & \\ & & & \mathbf{Q}_{\mathrm{u}}^{\mathrm{def,s}} & \\ & & & & \mathbf{R}_{\mathrm{u,bb}}^{\mathrm{R}} \end{bmatrix} \begin{Bmatrix} \boldsymbol{u}_{\mathrm{v}}^{\mathrm{RU}} \\ \boldsymbol{q}_{\mathrm{i}}^{\mathrm{RU}} \\ \boldsymbol{q}_{\mathrm{b}}^{\mathrm{RU}} \\ \boldsymbol{q}_{\mathrm{i}}^{\mathrm{R}} \\ \boldsymbol{q}_{\mathrm{b}}^{\mathrm{R}} \end{Bmatrix} + \begin{Bmatrix} \mathbf{0} \\ \boldsymbol{\mu}_{\mathrm{i}}^{\mathrm{RU}} \\ \boldsymbol{\mu}_{\mathrm{b}}^{\mathrm{RU}} \\ \boldsymbol{\mu}_{\mathrm{i}}^{\mathrm{R}} \\ \boldsymbol{\mu}_{\mathrm{b}}^{\mathrm{R}} \end{Bmatrix}$$

$$\begin{Bmatrix} \boldsymbol{g}_{\mathrm{v}}^{\mathrm{RU}} \\ \boldsymbol{m}_{\mathrm{i}}^{\mathrm{RU}} \\ \boldsymbol{m}_{\mathrm{b}}^{\mathrm{RU}} \\ \boldsymbol{m}_{\mathrm{i}}^{\mathrm{R}} \\ \boldsymbol{m}_{\mathrm{b}}^{\mathrm{R}} \end{Bmatrix} = \begin{bmatrix} \mathbf{I}_{\mathrm{vv}}^{\mathrm{RU}} & & & & \\ & \mathbf{Q}_{\mathrm{f}}^{\mathrm{def,s}} & & & \\ & & \mathbf{R}_{\mathrm{f,bb}}^{\mathrm{RU}} & & \\ & & & \mathbf{Q}_{\mathrm{f}}^{\mathrm{def,s}} & \\ & & & & \mathbf{R}_{\mathrm{f,bb}}^{\mathrm{R}} \end{bmatrix}^{H} \begin{Bmatrix} \boldsymbol{g}_{\mathrm{v}}^{\mathrm{RU}} \\ \boldsymbol{g}_{\mathrm{i}}^{\mathrm{RU}} \\ \boldsymbol{g}_{\mathrm{b}}^{\mathrm{RU}} \\ \boldsymbol{g}_{\mathrm{s}}^{\mathrm{R}} \\ \boldsymbol{g}_{\mathrm{b}}^{\mathrm{R}} \end{Bmatrix} \tag{16}$$

At this point, decoupling is performed using an extended interface. The advantage here is that the redundancy between the interface and the internal set of reduced DoFs is removed. However, the rigid dynamics of the internal DoFs are not involved in the decoupling. This may have a negative impact on the extended interface approach.

Note that as an alternative to the QR decomposition, one could extract a set of deformable representation vectors using the following relationship:

$$\mathbf{Q}_{\mathrm{u}}^{\mathrm{def}}(\omega) = (\mathbf{I} - \mathbf{R}_{\mathrm{u,ii}}^{\mathrm{R}} {\mathbf{R}_{\mathrm{u,ii}}^{\mathrm{R}}}^{+}) \mathbf{R}_{\mathrm{u,ii}}^{\mathrm{R}} \tag{17}$$

where the term $(\mathbf{I} - \mathbf{R}_{\mathrm{u,ii}}^{\mathrm{R}} {\mathbf{R}_{\mathrm{u,ii}}^{\mathrm{R}}}^{+})$ is an orthogonal projector onto the complement of the column space of $\mathbf{R}_{\mathrm{u,ii}}^{\mathrm{R}}$. The same holds for the extraction of the basis $\mathbf{Q}_{\mathrm{f}}^{\mathrm{def}}(\omega)$.

3.4 Enhanced VPT

Following the approach proposed in Section 3.3, yet another way to improve the VPT transformation technique is proposed here. The aim is to extend the VPT response and rigid reduction bases with a set of independent vectors extracted from measurements, which are able to represent the interface deformation. The first step of this procedure is to perform the SVD on the set of boundary FRFs $\mathbf{Y}_{\mathrm{bb}}^{\mathrm{R}}$ of the residual subsystem R:

$$\mathbf{Y}_{\mathrm{bb}}^{\mathrm{R}}(\omega) = \hat{\mathbf{U}}^{\mathrm{R}}(\omega) \hat{\mathbf{\Sigma}}^{\mathrm{R}}(\omega) (\hat{\mathbf{V}}^{\mathrm{R}}(\omega))^{H} \tag{18}$$

Then, the rigid transformation basis $\mathbf{R}_{\mathrm{u,bb}}^{\mathrm{R}}$ from the VPT and the full set of singular vectors $\hat{\mathbf{U}}^{\mathrm{R}}(\omega)$ are stacked column-wise in a matrix $\mathbf{C}$ to which the QR decomposition is applied:

$$\mathbf{C} = \left[\mathbf{R}_{\mathrm{u,bb}}^{\mathrm{R}} \middle| \hat{\mathbf{U}}^{\mathrm{R}}(\omega) \right] \qquad \Rightarrow \qquad \left[\mathbf{Q}_{\mathrm{u,b}}^{\mathrm{rigid}} \middle| \mathbf{Q}_{\mathrm{u,b}}^{\mathrm{def}}(\omega) \right] \mathbf{R} = \mathbf{C} \tag{19}$$

At this point, an orthonormal set of representation vectors is available, where the first 6 ones represent an orthonormal basis for the rigid IDMs, while the remaining vectors span the deformable motion of the

interface. One can therefore think of using a truncated basis $\mathbf{Q}^{\text{j}}_{\text{u,b}}$, formed by the full set $\mathbf{Q}^{\text{rigid}}_{\text{u,b}}$ and by j deformable vectors $\mathbf{Q}^{\text{def,j}}_{\text{u,b}}(\omega)$, to reduce the boundary dynamics so that both the rigid and the dominant deformable are represented. By doing so, the basis vectors for the space of rigid body motion at the interface are altered, meaning that it is no longer possible to ensure that they correspond to the six motions of a physical virtual point. Nevertheless, the resulting deformable basis $\mathbf{Q}^{\text{def,j}}_{\text{u,b}}(\omega)$ is still orthogonal to the rigid IDMs, i.e.:

$$\left(\mathbf{R}^{\text{R}}_{\text{u,bb}}\right)^{H}\mathbf{Q}^{\text{def,j}}_{\text{u,b}}(\omega) = \mathbf{0} \tag{20}$$

It follows that an extended VPT basis for response reduction can be constructed as follows:

$$\mathbf{Q}^{\text{j}}_{\text{u,b}} = \left[\ \mathbf{R}^{\text{R}}_{\text{u,bb}} \,\middle|\, \mathbf{Q}^{\text{def,j}}_{\text{u,b}}(\omega)\ \right] \tag{21}$$

The same process can be repeated for the force. The result is the following enhanced force reduction basis:

$$\mathbf{Q}^{\text{j}}_{\text{f,b}} = \left[\ \mathbf{R}^{\text{R}}_{\text{f,bb}} \,\middle|\, \mathbf{Q}^{\text{def,j}}_{\text{f,b}}(\omega)\ \right] \tag{22}$$

These bases can now be used within a decoupling approach where a standard interface is sufficient to preserve the deformable dynamics of the interface. However, the main assumption is that the interface is flexible, otherwise the retained singular vectors would only carry noise and measurement errors.
Note that to obtain the deformable representation vectors in $\mathbf{Q}^{\text{def}}_{\text{u,b}}(\omega)$ and $\mathbf{Q}^{\text{def}}_{\text{f,b}}(\omega)$, the QR decomposition here can be replaced by orthogonal projectors, similar to what is proposed in Section 3.3 (see Eq. (17)):

$$\mathbf{Q}^{\text{def}}_{\text{u,b}}(\omega) = (\mathbf{I} - \mathbf{R}^{\text{R}}_{\text{u,bb}}{\mathbf{R}^{\text{R}}_{\text{u,bb}}}^{+})\mathbf{R}^{\text{R}}_{\text{u,bb}} \qquad \text{and} \qquad \mathbf{Q}^{\text{def}}_{\text{f,b}}(\omega) = (\mathbf{I} - \mathbf{R}^{\text{R}}_{\text{f,bb}}{\mathbf{R}^{\text{R}}_{\text{f,bb}}}^{+})\mathbf{R}^{\text{R}}_{\text{f,bb}} \tag{23}$$

Moreover, instead of directly using the deformable representation vectors (despite the method employed to obtain them), they could be exploited to infer the residual dynamics on a set of extended geometrical VPT IDMs. The concept of extended geometrical IDMs is described in [17].
As a final remark, the approach proposed in this Section could also be applied to the whole set of DoFs $r = i \cup b$, improving the decoupling solution thanks to the large overdetermination of the interface.

4 Experimental application

To assess the advantages and drawbacks of the approaches proposed in Section 3 to weaken the decoupling, the same experimental measurements used in [14] are employed. The target benchmark is called the *AM* structure and represents the assembled system RU. It is composed of an *A*-shaped (unknown subsystem U) and of an *S*-shaped (residual subsystem R) aluminum components, which are joined together with an M10 hexagon head screw with a locking nut. To obtain the FRFs needed for the decoupling, three different roving hammer SIMO impact test campaigns are conducted separately on the assembled system RU (Fig. 3(a)), the residual subsystem R and the unknown subsystem U (Fig. 3(b)). This last one will be used to validate the results. The responses (accelerations) are measured with triaxial accelerometers. During the tests on RU and U, the unknown subsystem is connected to a vibration-free table through two cylindrical supports, as shown in Fig. 3(a). Instead, the residual subsystem is suspended with soft bungees to simulate free-floating conditions. A total of 9 accelerometers (2 on U and 7 on R) and 27 impact points (6 on U and 21 on R) are homogeneously distributed on the assembled system to fully control/observe all the relevant dynamics for the decoupling procedure. The set of measurement channels (blue arrows) and excitations (red arrows) is shown in Fig. 4, which also reports the DoF partitioning according to Section 2.1. Responses and excitations are placed in a collocated manner between RU and R. To perform the VPT, a virtual point is placed right in the middle of the connection region between R and U. Its DoFs play the role of the coupling DoFs c.

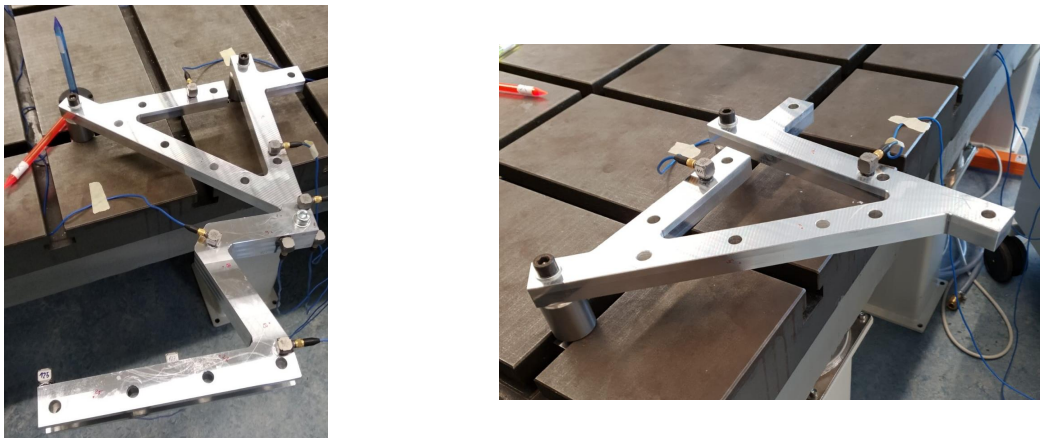

(a) Assembled system RU. (b) Unknown subsystem U.

Figure 3: Experimental measurement campaign on the different subsystem involved in the decoupling.

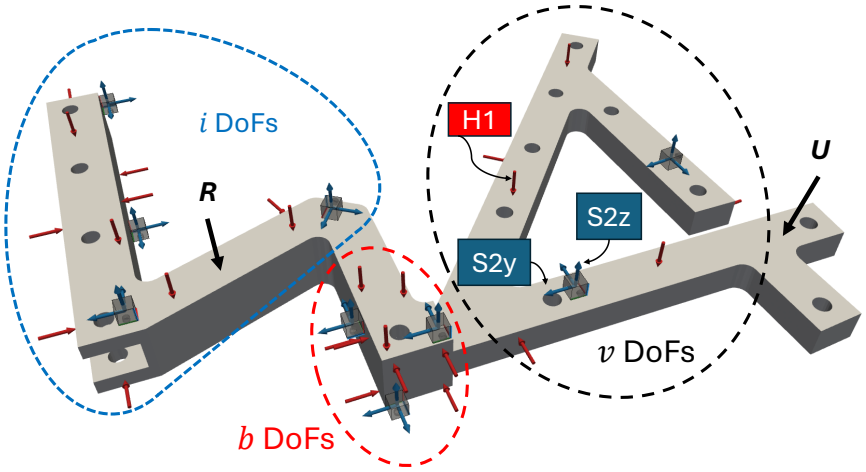

Figure 4: Response (blue arrows) and excitation (red arrows) DoFs selected on the assembled structure RU.

5 Results

In this Sections, the results obtained using the weakening methods proposed in Section 3 are presented and compared with other state-of-the-art approaches.

Fig. 5 shows the identified FRFs of the unknown subsystem U corresponding to its internal DoFs v (see Fig. 4), obtained with the combined VPT and SVT decoupling approach (blue line) presented in Section 3.1. The results are compared with those obtained using other well-established approaches, i.e. VPT with both standard (light green) and extended (dark green) decoupling interfaces and SVT (in red). The reference (directly measured) FRFs are also reported by the dashed black line. Notably, the VPT with the standard interface (light green line) is far from the true FRFs in different frequency ranges due to the impossibility of retaining the deformable interface motion. On the other hand, the results of the extended interface are highly scattered, indicating that the corresponding interface problem is ill-conditioned. Nevertheless, no regularization technique was used here to improve the conditioning of the interface problem. The latter result can be improved using the combined VPT and SVT approach proposed in Section 3.1. In particular, after observing the CMIF plot of the internal FRFs $\mathbf{Y}_{ii}^{R}$ shown in Fig. 6(a), only the first six singular vectors (not shaded) are used to reduce the responses and forces at the internal DoFs. In this way, measurement errors and noise at the internal DoFs are averaged, and only the relevant dynamics are included in the decoupling.

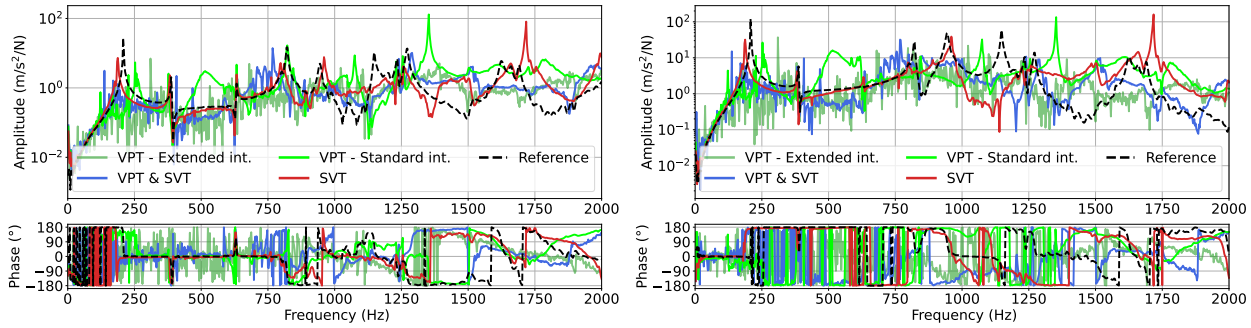

(a) $S2Y - H1$. (b) $S2Z - H1$.

Figure 5: Comparison of the resulting accelerance FRFs of the unknown subsystem U obtained with the VPT and SVT approach and other well-established methods. The measured FRF is reported by the dashed black line.

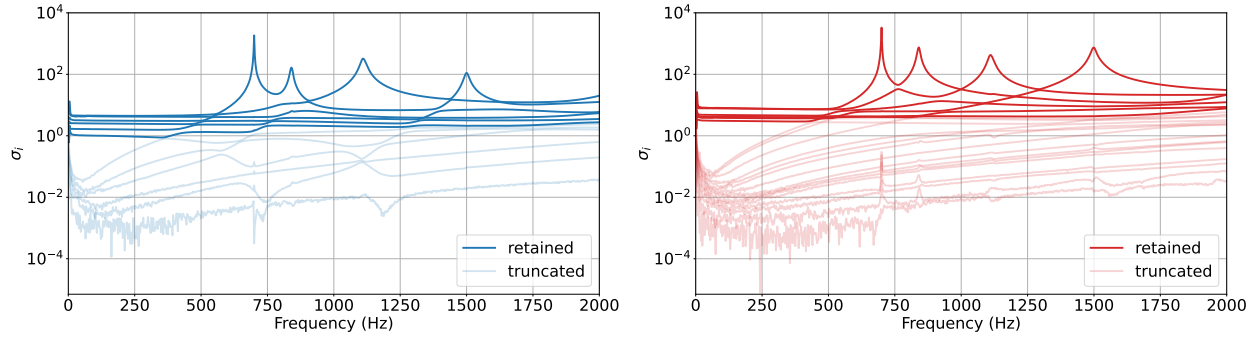

(a) $\mathbf{Y}^{\mathrm{R}}_{\mathrm{ii}}$. (b) $\mathbf{Y}^{\mathrm{R}}_{\mathrm{rr}}$.

Figure 6: CMIF plots used in the VPT and SVT (a) and in SVT (b) approaches. In both cases, only the first 6 singular values are retained.

Therefore, the scattering is reduced compared to the VPT with extended interface (dark green), although it is still significant at low frequencies. This may be due to the presence of redundant rigid dynamics introduced by the internal DoFs. Anyway, the ability to reconstruct the dynamic behavior of U is improved, although significant discrepancies remain for high frequencies. A sensitivity study on the VPT and SVT approach showed that the best results come from a compromise between a small amount (low redundancy/error) and a large amount (high flexible content) of retained singular vectors. However, it is not easy to find this balance manually.

Fig. 5 also shows that the SVT approach outperforms all other methods because it uses only the minimum amount of information required (extracted from a larger data set) within the decoupling, while allowing to maintain the flexibility of the interface. Again, six singular vectors were used to reduce the responses and forces at the DoFs r (boundary plus internal) of R, as suggested by the CMIF of $\mathbf{Y}^{\mathrm{R}}_{\mathrm{rr}}$ shown in Fig. 6(b).

In Section 3.2 the VPT and partitioned SVT approach was proposed. It is compared with the VPT and SVT one in Fig. 7, where only the first six singular vectors are retained in both cases. The two approaches seem to give similar results in the frequency range of interest.

To improve the conditioning of the IFM at low frequencies, the VPT and orthogonalized SVT approach proposed in Section 3.3 is applied. As shown in Fig. 8, the orthogonalization of the singular vectors $\tilde{\mathbf{U}}^{\mathrm{R}}$ and $\tilde{\mathbf{V}}^{\mathrm{R}}$ seems to allow the separation of the flexible internal dynamics from the rigid ones. Within the decoupling, compatibility and equilibrium are successively imposed on the VP DoFs and on the dynamics associated with the first s (here $s = 2$) deformable basis vectors. In this way, the rigid internal dynamics are not included in the IFM, thus avoiding redundancies with the rigid interface ones. The results obtained

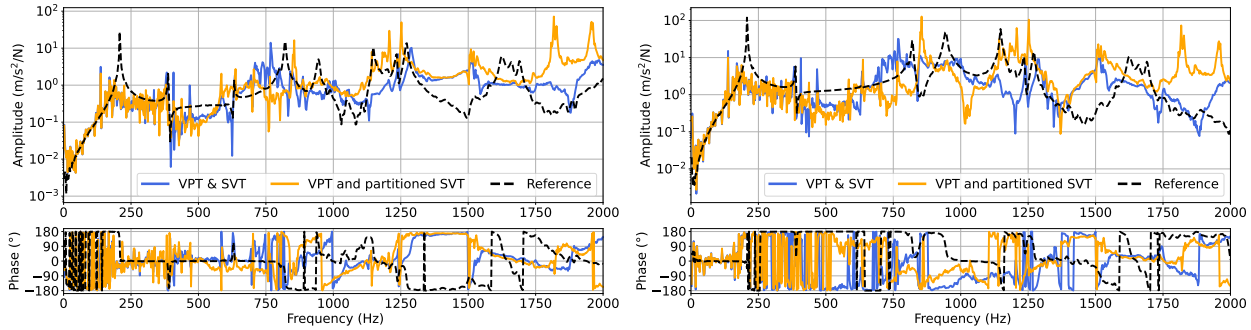

(a) $S2Y - H1$. (b) $S2Z - H1$.

Figure 7: Accelerance FRFs of the unknown subsystem U obtained with the "VPT and SVT" (Section 3.1) and "VPT and partitioned SVT" (Section 3.2) methods. The measured FRF is reported by the dashed black line.

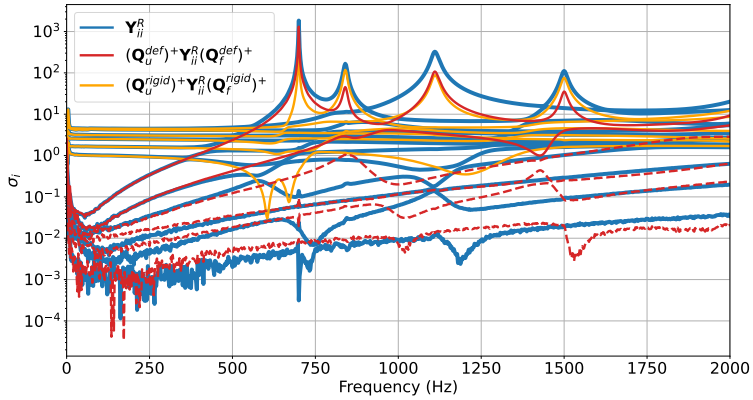

Figure 8: CMIF plot of the measured FRF matrix $\mathbf{Y}_{ii}^{R}$ and of the same matrix transformed with the deformable and rigid orthogonalized vectors.

with this approach are shown in Fig. 9 by the red line. There are only small improvements compared to the VPT solutions with standard interface (e.g. peak at 940 Hz). Compared to the SVT and VPT approaches (blue curve), the scattering is reduced in the mid-frequency range, but remains significant at low frequencies. Overall, removing the rigid contribution of the internal DoFs seems to remove much useful information for the reconstruction.

The condition number (CN) of the interface flexibility matrix for the compared reduction strategies is shown in Fig. 10. As expected, the CN of VPT and SVT with and without orthogonalization is lower than that of the VPT approach with extended interface, proving that they have better performances in terms of error propagation while still allowing to maintain the interface flexibility. On the other hand, the VPT and partitioned SVT approach have a higher CN over frequency than the VPT with extended interface. Notably, the conditioning of the SVT approach is much better, although the desired physical interface topology is lost.

Finally, the enhanced VPT approach proposed in Section 3.4 was tested on the benchmark structure using experimental data. However, the results were not in line with expectations, probably due to the lack of sufficient data at the interface to guarantee correct controllability/observability of the interface deformable dynamics.

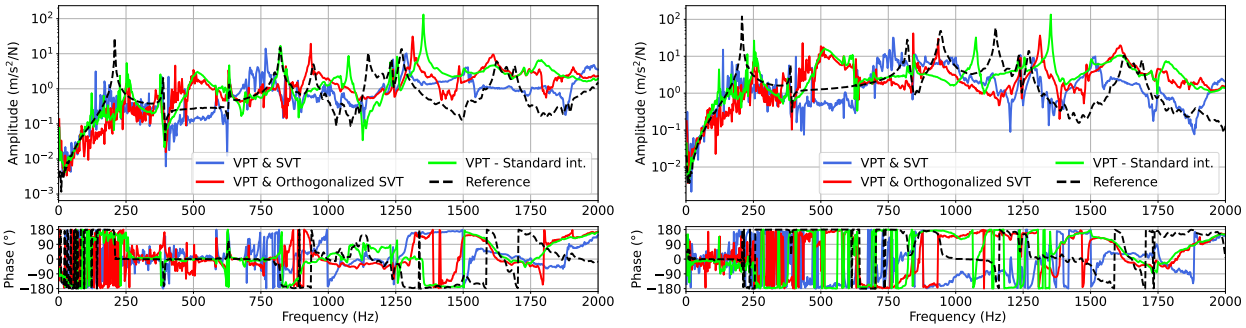

(a) $S2Y - H1$. (b) $S2Z - H1$.

Figure 9: Accelerance FRFs of the unknown subsystem U obtained with the "VPT and SVT" (Section 3.1) and "VPT and orthogonalized SVT" (Section 3.3) methods. The measured FRF is reported by the dashed black line.

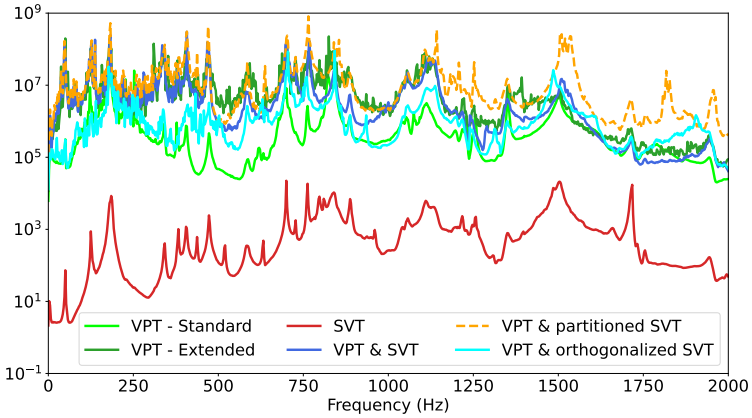

Figure 10: Condition number of the different procedure implemented.

6 Conclusions

In this paper, several approaches to weaken the decoupling compatibility conditions have been proposed. In applications where direct measurements at the interface between components are not possible, these methods allow the interface topology to be described in terms of physical translational and rotational coordinates, while providing improved substructure decoupling. The effectiveness of the proposed approaches was evaluated using experimental data of a laboratory benchmark.

Most of the proposed methods aim at improving the VPT with extended decoupling approach. The results show that the VPT and SVT approach successfully reduces the scatter in the solution. The VPT and partitioned SVT approach does not provide relevant improvements compared to the VPT and SVT one. The VPT and orthogonalized SVT successfully allow to improve the conditioning of the IFM with a consequent reduction of the scatter in the results, but this method needs further formalization. In addition, another approach, i.e. the enhanced VPT, has been proposed to improve decoupling while avoiding the extended interface concept. This could have positive impact on coupling procedures. However, this method did not give satisfactory results and needs further investigation in applications where interface flexibility is much more relevant.

References

[1] D. de Klerk, D. J. Rixen, and S. N. Voormeeren, "General Framework for Dynamic Substructuring: History, Review and Classification of Techniques," *AIAA Journal*, vol. 46, no. 5, pp. 1169–1181, 2008.

[2] J. Zhen, T. C. Lim, and G. Lu, "Determination of system vibratory response characteristics applying a spectral-based inverse sub-structuring approach. Part I: analytical formulation," *International journal of vehicle noise and vibration*, vol. 1, no. 1-2, pp. 1–30, 2004.

[3] J. W. R. Meggitt and A. T. Moorhouse, "In-situ sub-structure decoupling of resiliently coupled assemblies," *Mechanical Systems and Signal Processing*, vol. 117, pp. 723–737, 2019.

[4] W. D'Ambrogio and A. Fregolent, "Direct decoupling of substructures using primal and dual formulation," in *Linking Models and Experiments*, ser. Conference Proceedings of the Society for Experimental Mechanics Series, vol. 2, 2011.

[5] D. de Klerk, D. J. Rixen, and J. de Jong, "The Frequency Based Substructuring (FBS) Method reformulated according to the Dual Domain Decomposition Method," in *Proceedings of the 24th International Modal Analysis Conference, A Conference on Structural Dynamics*, 2006, pp. 1–14.

[6] W. D'Ambrogio and A. Fregolent, "Decoupling procedures in the general framework of frequency based substructuring," in *Proceeding of 27th International Modal Analysys Conference*, vol. 70. Society forExperimental Mechanics, Bethel, CT, 2009.

[7] S. N. Voormeeren and D. J. Rixen, "A Dual Approach to Substructure Decoupling Techniques," in *Structural Dynamics*, ser. Conference Proceedings of the Society for Experimental Mechanics Series, vol. 3. Springer, 2011, pp. 601–616.

[8] P. Sjövall and T. Abrahamsson, "Substructure system identification from coupled system test data," *Mechanical Systems and Signal Processing*, vol. 22, no. 1, pp. 15–33, 2008.

[9] S. N. Voormeeren and D. J. Rixen, "A family of substructure decoupling techniques based on a dual assembly approach," *Mechanical Systems and Signal Processing*, vol. 27, pp. 379–396, 2012.

[10] W. D'Ambrogio and A. Fregolent, "Substructure decoupling as the identification of a set of disconnection forces," *Meccanica*, vol. 52, no. 13, pp. 3117–3129, 2017.

[11] M. V. van der Seijs, D. van den Bosch, D. J. Rixen, and D. de Klerk, "An improved methodology for the virtual point transformation of measured frequency response functions in dynamic substructuring," in *4th ECCOMAS Thematic Conference on Computational Methods in Structural Dynamics and Earthquake Engineering (COMPDYN)*, vol. 4, Greece, 2013, pp. 4334–4347.

[12] M. S. Allen, D. Rixen, M. Van der Seijs, P. Tiso, T. Abrahamsson, and R. L. Mayes, *Substructuring in Engineering Dynamics*, ser. CISM International Centre for Mechanical Sciences. Springer Cham, 2020.

[13] D. Ocepek, F. Trainotti, G. Čepon, D. J. Rixen, and M. Boltežar, "On the experimental coupling with continuous interfaces using frequency based substructuring," *Mechanical Systems and Signal Processing*, vol. 217, p. 111517, 2024.

[14] F. Trainotti, T. Bregar, S. W. B. Klaassen, and D. J. Rixen, "Experimental decoupling of substructures by singular vector transformation," *Mechanical Systems and Signal Processing*, vol. 163, p. 108092, 2022.

[15] W. D'Ambrogio and A. Fregolent, "Promises and pitfalls of decoupling procedures," in *Proceeding of 26th International Modal Analysys Conference*. Society forExperimental Mechanics, Bethel, CT, 2008.

[16] G. Strang, "Computational science and engineering," *Optimization*, vol. 551, no. 563, 2007.

[17] E. A. Pasma, M. V. van der Seijs, S. W. B. Klaassen, and M. W. van der Kooij, "Frequency Based Substructuring with the Virtual Point Transformation, Flexible Interface Modes and a Transmission Simulator," in *Dynamics of Coupled Structures*, ser. Conference Proceedings of the Society for Experimental Mechanics Series, A. Linderholt, M. Allen, R. Mayes, and D. Rixen, Eds., vol. 4. Cham: Springer, 2018, pp. 205–213.